Cooling dynamics of carbon cluster anions

H Shiromaru[1]**, T Furukawa**[2]**, G Ito**[2]**, N Kono**[2]**, H Tanuma**[2]**, J Matsumoto**[1]**, M Goto**[1,3,4]**, T Majima**[5]**, A E K Sundén**[3]**, K Najafian**[3]**, M. S. Pettersson**[3]**, B. Dynefors**[6]**, K Hansen**[3]**, T Azuma**[4]

[1] Dept. Chem., Tokyo Metropolitan Univ. Hachioji 192-0397, Japan
[2] Dept. Phys., Tokyo Metropolitan Univ. Hachioji 192-0397, Japan
[3] Dept. Phys., Univ. Gothenburg, 41296 Gothenburg, Sweden
[4] AMO Physics Laboratory, RIKEN, Wako 351-0198, Japan
[5] Quantum Sci. Eng. Center, Kyoto Univ., Uji 611-0011, Japan
[6] Appl. Phys., Chalmers Technical Univ., 41296 Gothenburg, Sweden。

E-mail: shiromaru-haruo@tmu.ac.jp

Abstract. A series of ion storage experiments on small carbon cluster anions was conducted to understand size-dependent cooling processes. The laser-induced delayed electron detachment time profile show clear even/odd alternation due to the presence of the electronic cooling. The time evolution of the internal energy distribution was simulated for C_n^- (n=4 to 7) with a common procedure taking vibrational and electronic cooling into account.

1. Introduction

Recently, we reported a series of studies on laser-induced electron detachment of carbon cluster anions using an electrostatic ion storage ring to understand the cooling behaviour of high-temperature anions [1-6]. For the clusters C_n^- (n = 4 - 7), neutral species (C_n) produced by delayed electron detachment were detected, probing the time-profile of the photo-induced delayed neutral yield as a function of the time after photo-excitation, and the storage time (laser firing time) dependence of the total yield. In these papers, we have shown how to obtain information on the internal energy distribution from the data. Generally, within the uncertainty involved in the measurements and the theoretical approaches, the delayed detachment (vibrational auto-detachment) and radiative cooling of these anions are well explained by statistical considerations taking account of molecular vibrations and electronic structures, without the need to introduce any electronic metastable states. The radiative cooling rates show a strong even/odd alternation, which is due to the presence/absence of a contribution from the fast electronic cooling p rocesses [2,3,4,6].

A schematic view of the energy distribution of hot anions undergoing radiative cooling and vibrational auto-detachment is shown in Fig.1. Above the detachment threshold, auto-detachment with a rate constant k_d competes with radiative cooling. Observation of the time profile of the neutral yields, $I(t)$, gives information on the mechanism of radiative cooling. In the ion storage study, the anions with larger internal energy are preferentially removed from the ring, resulting in cooling of the ensemble of

stored anions. This process is referred to as depletion cooling. For odd-numbered cluster anions, the time profile of the neutral yields after photo-excitation is governed by the competition between electron detachment (depletion cooling) and vibrational radiative cooling, of which the former plays a dominant role above the detachment threshold. Since the experiments explored hot anions with broad energy distribution, the change in the population with the internal energy (E) is much slower than that of k_d. A characteristics of the depletion cooling under such conditions is the power law decay represented by $I(t) \propto t^{-\gamma}$, where γ is close to one. On the other hand, for even-numbered cluster anions, electron detachment is strongly suppressed by fast radiative cooling due to electronic transitions *via* thermally populated electronic excited states, so called "recurrent fluorescence". Since the population above the detachment threshold decreases quickly, the $I(t)$ decays quickly, providing a sign of electronic cooling.

Below the detachment threshold, odd-numbered cluster anions are slowly cooled by vibrational radiative cooling, whereas even-numbered ones continue to be cooled by electronic radiative cooling as long as they have an excitation energy somewhat higher than that of the relevant electronic excited state. Delayed detachment after photo-excitation can give information on the cooling in this energy region, since the detachment yield at a specific time after photo-excitation probes the population at a specific energy before photo-excitation, as will be shown later.

The characteristic cooling behaviour of carbon cluster anions is one of the consequences of the electronic structures which show a well-known periodicity; the ground states of even-numbered clusters are triplets while the odd-numbered are singlets, as illustrated in Fig. 2 [7]. This is the origin of the even/odd alternations observed in abundance, reactivity, and so on, both for neutral and ionic carbon clusters. The even/odd alternation is superimposed on the smooth size dependence of the molecular property. For example, the electron affinity (E_a) of the neutral cluster is higher for even-numbered ones and systematically increases with the size [8, 9]. The energy levels of the excited states of anions and the E_a of corresponding neutrals are shown in Table I for C_4^- - C_7^-. As can be seen in the Table, the E_a of C_4 (small, even-numbered) is not so different from that of C_7 (large, odd-numbered). The energy of the dipole allowed low-lying excited states tends to be smaller for the even-numbered and the larger anions. This is the key factor that determines whether the electronic cooling works. The efficiency of the electronic cooling is determined by the relative values of the detachment threshold ($= E_a$) and electronic excitation energy
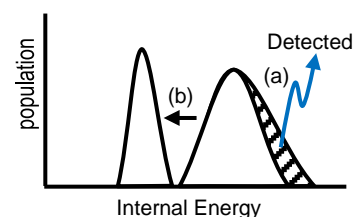
Figure 1. Generic energy distribution of hot anions. (a) The hatched area indicates depletion by detachment, in which anions will be detected as neutral products. (b) Radiative cooling does not yield the neutrals while it still accelerates the decrease of them with the time.

$:C=C=C:$ $(1\pi_u)^4$

$:C=C=C=C:$ $(1\pi_u)^4(1\pi_g)^2$
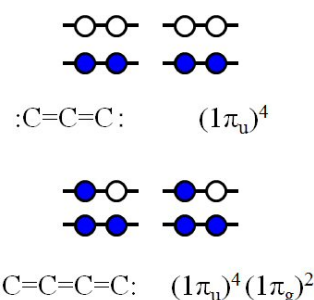
Figure 2. Schematic energy diagram of odd-numbered (C_3 as an example) and even-numbered (C_4) carbon clusters. Odd numbered cluster has 4n π electrons which fully occupy the degenerate HOMO, whereas even-numbered cluster has 4n+2 π electrons which occupy the half of the HOMO.

Table I. The term symbols of the ground and the dipole allowed electronic excited states of C_4^- - C_7^- and the excitation energies in eV. Those for neutral clusters and the E_a values in Ref. [9] are also shown.

C_4^-	[10,11]	C_5^-	[12]	C_6^-	[10, 11]	C_7^-	[12]
$X^3\Sigma_g^-(C_4)$	3.88(E_a)	$X^1\Sigma_g^+(C_5)$	2.85(E_a)	$X^3\Sigma_g^-(C_6)$	4.18(E_a)	$X^1\Sigma_g^+(C_7)$	3.36(E_a)
$C^2\Pi_u$	2.71	$A^2\Pi_g$	2.50	$C^2\Pi_g^+$	2.04	$B\Pi_u$	2.52
$B^2\Sigma_u^+$	1.34	$X^2\Pi_u$	0	$A^2\Sigma_g^+$	1.16	$A^2\Pi_u$	1.98
$X^2\Pi_g$	0			$X^2\Pi_u$	0	$X^2\Pi_g$	0

of the dipole allowed states, and the transition probability.

In this paper, we will show that the cooling processes of both even- and odd-numbered carbon cluster anions can be treated by a common procedure based on a purely statistical description. The vibrational and electronic radiative cooling rate constants, denoted by k_v and k_e, respectively, are defined as the transition probability per second. Since the emitted energy per transition is very different for the electronic and the vibrational transitions, the cooling rates dE/dt will increase dramatically if the electronic cooling is present.

2. Experimental results

The experiments were performed using an electrostatic ion storage ring at Tokyo Metropolitan University (TMU E-ring) [13], of which a schematic view is shown in Fig. 3, together with a timing chart shown on the right. Carbon cluster anions were produced with a laser ablation source or a Cs sputter source, and injected into the ring with energies of 15 or 20 keV. Cooling gases were not employed. The hot cluster anions were gradually cooled during storage, both by depletion and radiative cooling, and then they were reheated by a pulsed laser merged in one of the straight sections of the ring. As shown in the timing chart (a) in the right of Fig. 3, the stored ion bunch periodically passed through this straight section. The timing of the laser irradiation was adjusted to a specific turn of the bunch, as shown in the timing chart (b). The neutral particles generated one or a half revolution after laser irradiation were detected by microchannel plate detectors (MCP) located at the extension of the lower and upper straight sections, shown in the timing chart (c) and (d), respectively. If the photo-excited ions have too much internal energy either because of too much energy before photo-excitation or of contribution of multi-photon absorption, detachment occurs only at the lower straight section. Such a fast detachment component, including one by prompt detachment, contributes only to the first peak in (c). The other peaks in (c) and (d) are due to delayed detachment exclusively.

With this experimental configuration, the anions within a specific range of lifetimes (several tens of microseconds depending on the masses and kinetic energies) were selectively detected. That is, we detected ions with a specific internal energy region, which is referred to as an energy window (E_0). For the small carbon cluster anions examined in the present study, the k_d is a rapidly varying function of the internal energy. The energy spread of E_0 is fairly narrow and located just above the detachment threshold. Thus, the neutralization yield summed over the laser-induced peaks (total neutral yield) is proportional both to the population at $E = E_0 - h\nu$ before photo-excitation and to the photo-absorption cross section. During the storage, below-threshold ions cool radiatively. The plot of the total neutral yield (y) versus cooling time (laser firing time, t_{las}) for fixed $h\nu$ gives the time evolution of the population at $E_0 - h\nu$.

The normalized decay profiles $I(t)$, the plots of the yields versus times after excitation, are shown in
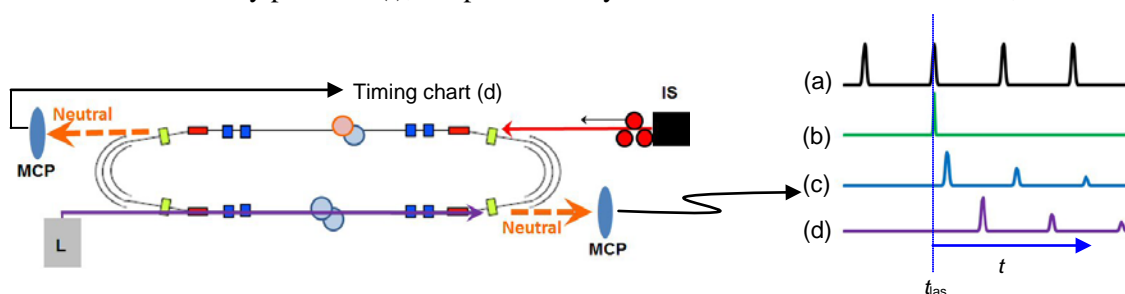
Figure 3. Schematic drawing of the experimental setup. The TMU E-ring comprises 16 components of ion optics indicated by rectangles. (IS) Ion sources of carbon cluster anions. Laser ablation or Cs-sputtering of graphite was employed. (L) Pulsed OPO laser pumped by YAG laser. To excite anions, the OPO laser was merged in the lower straight section in the figure. The timing chart indicates (a) the timing of the ion bunch passing in the laser merging side, (b) the timing of laser firing (t_{las}), (c) the time profile of neutral yields, $I(t)$, measured by the MCP in laser-merging side, and (d) that by the MCP in opposite side.

Figs. 4(a)-(d) for C_4^- to C_7^-. Aside from the absolute yield, the decay profiles are nearly independent of the excitation energy and the laser firing time for all the clusters. The data for C_5^- and C_7^- follow a power law indicating that these result from depletion cooling. The delayed detachment continues at least 10 revolutions after photo-excitation. On the other hand, the decay profiles for C_4^- and C_6^- are near single-exponential with much smaller time constants, indicating that these decays are strongly influenced by electronic radiative cooling of the laser-heated anions.
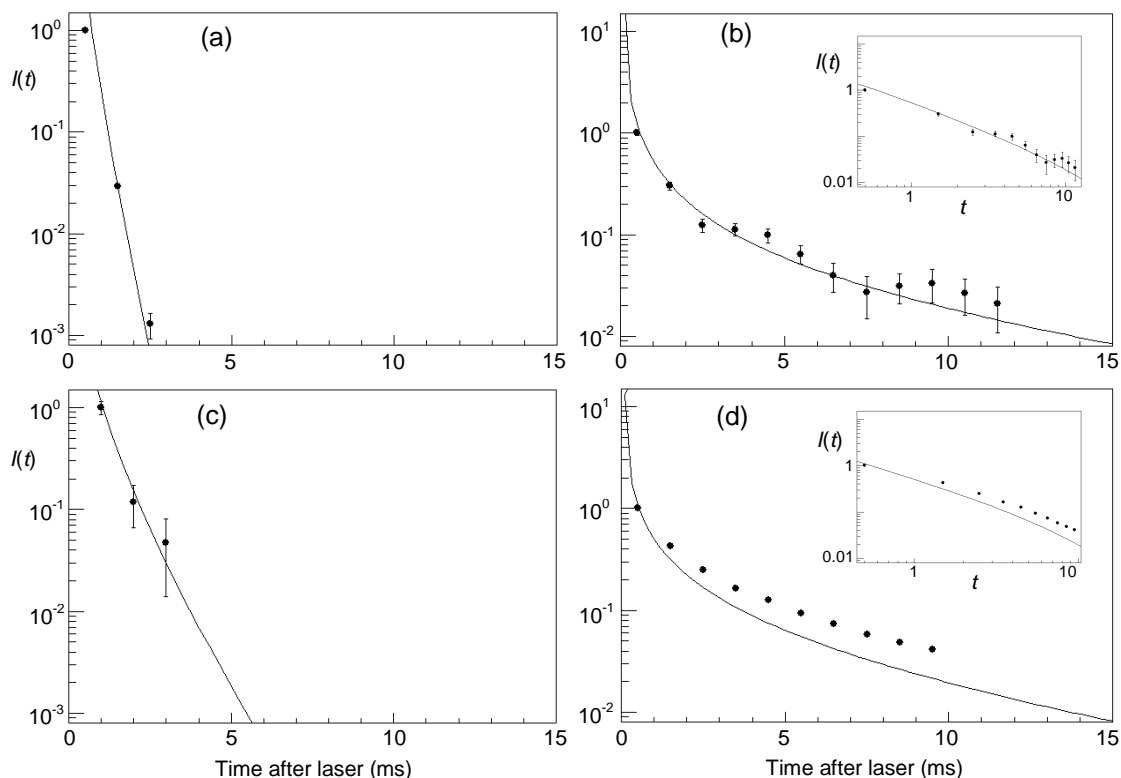
Figure 4. The neutral yields (normalized at the first data point) after photo-excitation. The lines indicate the simulated $I(t)$. The error bars in (a) – (c) represent standard deviation (1σ) of the independent runs. The error bars in (d) represent statistical uncertainties, which are smaller than the symbols. The revolution periods (time intervals of the plots) are 31.6, 35.3, 33.55, 46.0 μs for C_4^- to C_7^-. Note that the ion kinetic energies are not the same. The photon energies and the laser firing times are as follows: (a) C_4^-, $h\nu$=3.49 eV, t_{las} = 5 ms. (b) C_5^-, $h\nu$=2.58 eV, t_{las} = 30 ms. (c) C_6^-, $h\nu$=3.49 eV, t_{las} = 5 ms. (d) C_7^-, averaged over $h\nu$=2.70 eV at t_{las} = 6 - 18 ms, 2.40 eV at 4 - 13 ms, 2.10 eV at 3 - 10 ms. The inset figures in (b) and (d) show the same data in double logarithmic scale. The C_6^- data at the 3rd revolution involves large uncertainty but the near-exponential decay is confirmed by Chandrasekaran et al [14].

Plots of the total yield against the laser firing times (t_{las}) are shown in Fig. 5 (a)-(d) for C_4^- to C_7^-. For C_5^- and C_7^-, the yields initially go up and later go down, and the peak positions shift with the laser wavelengths. Excitation by longer wavelength light gives a curve that peaks at earlier storage time. This is consistent with the aforementioned energy window picture. If the cooling is vibrational, the population at $E_0 - h\nu$ is determined by the balance of the anions leaving from the $E_0 - h\nu$ region and those arriving from the higher energy region. If the maximum of the population locates at higher energy side of $E_0 - h\nu$ at the beginning of storage, the initial population change driven by vibrational radiative cooling results in increase of the population at that energy. As t_{las} proceeds, population reaches the maximum and further vibrational radiative cooling lowers the population. Since the red light samples the population at higher internal energies, the yield starts decreasing faster.

In strong contrast to this behaviour, the total yield for C_6^- shown in (c) monotonically decreases with increasing storage time, indicating that the maximum of the population is located at the lower energy side of $E_0 - h\nu$ (= 0.9 eV) from the start. That is, C_6^- is cooled significantly during the drift from the hot ion source to the ring, due to fast electronic cooling. The slow decrease of the total yield is explained by vibrational cooling in this energy region. For C_4^- shown in (a), the decrease is much faster (note the different time scales), especially for excitation by longer wavelength light, and the decay profiles are near single-exponential. This is understandable considering the large amount of energy taken away by a single electronic transition. Since there is no source of anions to replace the lost anions, the population at $E_0 - h\nu$ simply decreases with a rate governed by the electronic cooling rate at that energy. Since the k_{el} is nearly constant within the narrow energy window, the population follows a near single exponential decay. Then, on the basis of the above-mentioned simple model of the energy window, near-exponential decay of $y(t_{las})$ for C_4^- is rationalized.
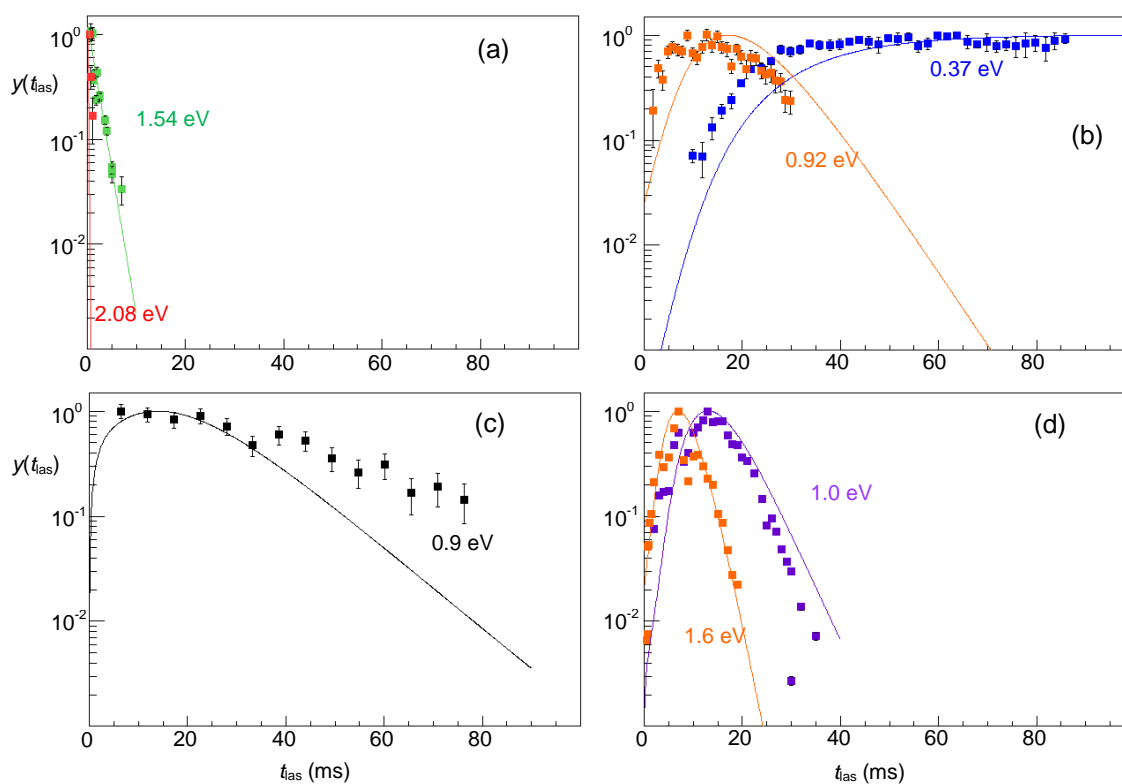
F igure 5. The total yield (y, arbitrary scale) as a function of laser firing time (t_{las}) for (a) C_4^-, $h\nu$=1.80 (red) and 2. 34 (green) eV, (b) C_5^-, $h\nu$=2.03 (orange) and 2.58 (blue) eV, (c) C_6^-, $h\nu$=3.49 eV, (d) C_7^-, 2.1 (orange) and 2. 7 (purple) eV. The error bars in (a) – (c) represent standard deviation (1σ) of the independent runs. The error ba rs in (d) represent statistical uncertainties, which are smaller than the symbols. The values of $E_0 - h\nu$ are in dicated in the figures.

3. Simulated cooling features

Since the detailed procedure of the simulation is presented in [5], we will present only an outline as well as the adopted molecular constants available from the literature. A flow chart of the simulation of the depletion cooling and radiative cooling processes is shown in Fig. 6. The vibrational level density $\rho(E)$ was calculated with the Beyer-Swinehart algorithm [15] adopting the vibrational wavenumbers

from the literature and the harmonic oscillator approximation. The rate constant of electron detachment k_d is given by the detailed balance theory.
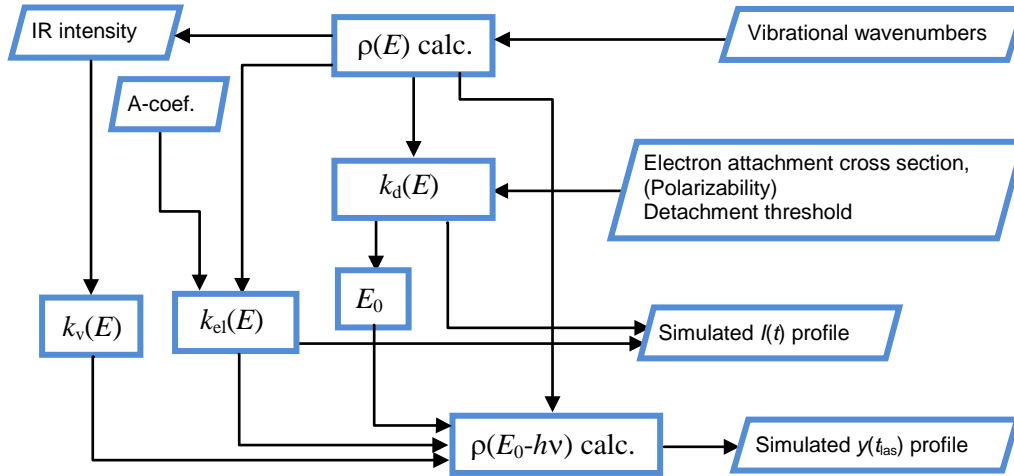
Figure 6. Flow chart for the simulation of the cooling processes. The input data are listed in Table II, and the outputs are compared with the experimental results.

$$k_d(E) = \int_0^{E - E_a} \frac{2m}{\pi^2 \hbar^3} \sigma(\varepsilon)\varepsilon \frac{\rho_d(E - E_a - \varepsilon)}{\rho_p(E)} d\varepsilon \,,$$

where E_a, m, ρ_p, ρ_d, ε are the electron affinity, mass of an electron, level densities of the parent (anion) and the daughter (neutral), kinetic energy of the detached electron. The term $\frac{2m}{\pi^2 \hbar^3}\sigma(\varepsilon)\varepsilon$ is the statistical weight of the free electron with the energy ε and the attachment cross section $\sigma(\varepsilon)$ [16]. The spin and orbital multiplicities of the parent and daughter are included in the ρ values. The $\sigma(\varepsilon)$ is approximated by the Langevin cross section derived from the literature value of polarizability (α), that is, $\sigma(\varepsilon) = \sigma_0 \varepsilon^{-1/2} = (2\alpha / \varepsilon)^{1/2}$. The vibrational radiative cooling rate constant k_v is calculated from the transition probabilities and statistical weights of the relevant vibronic states.

$$k_v^i(E) = A_{1-0}^i \frac{1}{\rho(E)} \sum_n n\rho_i(E - nh\nu_i) \,,$$

where $A_{1-0}^i, n, h\nu_i$ are the A-coefficient for the 0 to 1 vibrational transition, the vibrational quantum number, and the energy of the single transition of the mode i. The total vibrational cooling rate is given by

$$dE/dt = \sum_i h\nu_i k_v^i(E) \,.$$

The electronic cooling rate constant $k_{el}^i(E)$ and the corresponding cooling rate dE/dt are given by

$$k_{el}^i(E) = A_{el}^i \frac{\rho(E - h\nu_{el}^i)}{\rho(E)} \,, \quad dE/dt = \sum_i h\nu_{el}^i k_{el}^i(E) \,, \text{ respectively, where } A_{el}^i \text{ is the A-coefficient for the}$$

electronic transition from the excited state i, $h\nu_{el}^i$ is the electronic excitation energy, $\rho(E)$ is the vibrational level density of the electronic ground state, $\rho(E - h\nu_{el}^i)$ is that of the electronic excited state.

We use the approximation that the vibrational wavenumbers are the same for the electronic ground and the excited states.

The initial energy distribution of the ions in the source was calculated assuming a thermal distribution with a temperature of 5000 K, which is an arbitrary but reasonable value. The time evolution of the distribution was calculated using the above cooling rates. Thermally populated electronic excited states were taken into account by statistical sharing of the internal energy by the vibrational modes both in the electronic ground and the excited states. The energy distribution curve before photo-excitation was shifted upward by $h\nu$ after photo-excitation. Then, considering the k_d, k_v and k_{el}, the neutral yield against the time after laser excitation, $I(t)$, was simulated. The neutral yield at the storage time, $y(t_{las})$, was given by the population at the $E_0 - h\nu$ region, taking the detachment probability at the detection time window into account.

The molecular constants employed in the simulation are listed in Table II, whereas the reported values of the E_a and $h\nu_{el}$ are shown in Table I. The theoretical values of the polarizabilities are given in a.u. [17], which are converted to σ_0 in eV. Although the uncertainty in the σ_0 is rather large, it does not affect our simulation significantly, since the k_d is a linear function of σ while the level density ρ varies very rapidly with energy. The vibrational wavenumbers of the neutral carbon clusters are adopted from recent theoretical calculations [18]. Those for the anions are from measurements in a cold matrix [19]. The A-coefficients of the IR emissions for the anions are converted from the IR intensities given in parentheses. The time windows were calculated using the ion's revolution periods, and were converted to the energy windows (E_0) according to the calculated k_d. The obtained E_0 values for C_4^- - C_7^- are 3.88 eV ($\cong E_a$), 2.95 eV ($\cong E_a + 0.1$ eV), 4.4 eV ($\cong E_a + 0.2$ eV), 3.7 eV ($\cong E_a + 0.3$ eV). The

Table II. Molecular constants employed for simulation.

	C_4	C_5
α(a.u), $\sigma_0(\text{Å}^2)$ [17]	52.6, 47	71.7 , 55
Vibrational wavenumbers for neutrals (cm^{-1})[18].	2116, 1584, 931,336*, 159*	2253, 2027,1480, 790 ,552*, 222*,114*
Vibrational wavenumbers (cm^{-1}), IR intensities for anions (km/mol)[19].	2112.7 (0), 1785.2 (87), 926.4 (0), 605.4 (0), 533.1 (0), 265.5 (27), 241.5 (50)	1923.7 (0), 1902.5 (855), 1472.6 (23), 777.2 (0), 751.7 (0), 604.9 (8), 432.6 (0), 360.7 (0), 170.9 (35), 167.8 (24)
Oscillator strength for the electronic transition [20,21]	C-X 2.32×10^{-2} , $4{,}2\times10^{-2}$ B-X 3×10^{-3}	A-X 1.64×10^{-5}

	C_6	C_7
α(a.u), $\sigma_0(\text{A}^2)$ [17]	100, 65	127, 73
Vibrational wavenumbers for neutrals (cm^{-1})[18].	2179,2024,1721,1219, 665,467*,359*,197*,97*	2245,2209,1971,1597, 1105, 630*,583, 514*, 255*, 161*, 73*
Vibrational wavenumbers (cm^{-1}), IR intensities for anions (km/mol)[19].	127 (0.1394), 133 (0.1223), 285 (0), 293 (0), 517 (0.924), 553 (0.2643), 658 (0), 775 (0), 811 (0), 1222 (0.430), 1865 (0), 2037 (867.85), 2193 (0)	2079.6 (0), 1990.1 (157), 1835.7 (2331), 1608.7 (0), 1089.9 (8), 929.1 (2), 827.7 (3), 669.4 (0), 582.0 (0), 577.8 (0), 416.3 (8), 367.4 (12), 226.4 (0), 221.1 (0), 94.6 (20), 93.6 (23)
Oscillator strength for the electronic transition [20, 22]	C-X 0.3137, 3.73×10^{-2} A-X 3.2×10^{-3}	B-X 6.79×10^{-3} A-X 1.85×10^{-4}

The degenerate vibrational modes are indicated by the asterisk.

values of oscillator strength for the electronic transitions, cited from theoretical evaluations [20-22], are tabulated in the bottom row.

The simulated $I(t)$ and $y(t_{las})$ curves are indicated by solid lines in Figs. 4 and 5. Except for the oscillator strength of the B-X transition of C_4^-, which is increased by a factor of 5 from the literature value, fitting parameters are not employed. As demonstrated in the figures, agreement is quite satisfactory considering many approximations imposed in our simulations.

4. Conclusion

We have shown that the radiative cooling of small carbon cluster anions are well reproduced by simulations based on a purely statistical model. It should be noted that the simulation is based on the imposed approximation (Langevin cross section, harmonic oscillator, ignoring rotational states, and so on) and the values listed in Table II. For better quantitative agreement, a drastic improvement of the theoretical framework to treat hot molecules, which are rather floppy and undergoing molecular vibrations with a picture far different from harmonic, is needed. Experimentally, case-by-case approach gives additional information. For C_5^- and C_7^-, the fact that the $y(t_{las})$ curves measured at various $h\nu$ are scalable with respect to t_{las} helps us to derive the radiative cooling rates [2,3]. For even-numbered cluster anions, detection of the photons emitted in the electronic cooling process will open a new venue for radiative cooling studies [23].

References
[1] M. Goto *et al* 2013 *Phys. Rev.* **A 87** 033406
[2] M. Goto *et al* 2013 *J. Chem. Phys.* **139** 054306
[3] K. Najafian *et al J. Chem. Phys.* **140** 104311
[4] G. Ito *et al* 2014 *Phys. Rev. Lett.* **112** 183001
[5] T. Furukawa *et al* 2015 *Nucl. Instr. and Meth.* **B 354,** 192
[6] N. Kono *et al* 2014 *Phys. Chem. Chem. Phys.,* in press.
[7] A. van Orden, R. J. Saykally 1998 *Chem. Rev.* **98**, 2313.
[8] Yang et al., 1988 *Chem. Phys. Lett.* **144**,431.
[9] D. W. Arnold *et al* 1991 *J. Chem. Phys.* **95**, 8753.
[10] Y. Zhao *et al* 1996 *J. Chem. Phys.* **105**, 4905.
[11] P. Freivogel *et al* 1997 *J. Chem. Phys.* **107**, 22.
[12] D. Forney *et al* 1997 *J. Phys. Chem.* **A 101**, 5292.
[13] S. Jinno *et al* 2004 *Nucl. Instrum. Meth. Phys. Res.* **A 532** 477.
[14] V. Chandrasekaran et al., 2014 *J. Phys. Chem. Lett.* **5** 4078.
[15] T. Beyer, D. F. Swinehart, 1973 *Commun. ACM* **16** 379.
[16] K. Hansen "Statistical Physics of Nanoparticles in the Gas Phase" 2011 Springer Series on Atomic, Optical, and Plasma Physics.
[17] P. Fuentealba 1998 *Phys. Rev.* **A 58,** 4232.
[18] H. Do, N. A. Besley 2015 *Phys. Chem. Chem. Phys.* **17** 3898.
[19] J. Szczepanski *et al* 1997 *J. Chem. Phys.* **A 101** 1841.
[20] X.-G. Guo *et al* 2011 *J. Comp. Chem.* **5**, 93.
[21] K. Takahashi, private communication, Z. Cao, private communication.
[22] Z. Cao, S. D. Peyerimhoff 2001 *J. Phys. Chem.* **A 105** 627.
[23] Y. Ebara *et al*., to be published.